Meeting the Requirements to Deploy Cloud RAN over Optical Networks

L. Velasco, A. Castro, A. Asensio, M. Ruiz, G. Liu, C. Qin, R. Proietti, and S. J. B. Yoo

***Abstract*—Radio Access Network (RAN) cost savings are expected in future Cloud RAN (C-RAN). In contrast to traditional distributed RAN architectures, in C-RAN, Remote Radio Heads from different sites can share baseband processing resources from virtualized Base Band Unit pools placed in a few central locations (CO). Due to the stringent requirements of the several interfaces needed in C-RAN, optical networks have been proposed to support C-RAN. One of the key elements that need to be considered are the optical transponders. Specifically, Sliceable Bandwidth-Variable Transponders (SBVT) have recently shown many advantages for core optical transport networks. In this paper, we study the connectivity requirements of C-RAN applications and conclude that dynamicity, fine granularity, and elasticity are needed. However, there is no SBVT implementation that supports those requirements and thus, we propose and assess an SBVT architecture based on Dynamic Optical Arbitrary Generation / Measurement (DOAWG / DOAWM). We consider different Long Term Evolution–Advanced (LTE-A) configurations and study the impact of the centralization level in terms of Capital Expense and Operating Expense (CAPEX and OPEX): an optimization problem is modeled to decide which COs should be equipped and the equipment, including transponders, needs to be installed. Results show noticeable cost savings from installing the proposed SBVTs compared to installing fixed transponders. Finally, compared to the maximum centralization level, remarkable costs savings are shown when a lower level of centralization is considered.**

***Index Terms*—5G mobile/wireless convergence, Cloud RAN, Elastic Optical Networks, Sliceable transponders.**

I. Introduction

Radio access technologies evolution and centralized Radio Access Networks (RAN) architectures ([2], [3]) reveal new paradigms in next generation mobile networks. The commercial availability of technologies such as Long Term Evolution (LTE) requiring high capacity and strict delay constraints for complex coordination schemes among their base stations and the ever increasing Total Cost of Ownership (TCO) in mobile networks (including both Capital Expenditures (CAPEX) and Operational Expenditures (OPEX)) to satisfy the expected cell site's demand increment [3], [4] motivate research towards centralized RAN architectures. We refer the reader to the studies in [5] and [6] regarding advances in centralized RAN.

Manuscript received September 30, 2016. This work was presented in part at ONDM [1].

Luis Velasco (lvelasco@ac.upc.edu), Adrian Asensio and Marc Ruiz are with the Optical Communications Group (GCO) at Universitat Politècnica de Catalunya (UPC), Barcelona, Spain.

Alberto Castro, Gengchen Liu, Chuan Qin, Roberto Proietti, and S. J. Ben Yoo are with the University of California (UC Davis), Davis, USA.

Among the main factors contributing to CAPEX increase are the need to deploy more base stations, new building locations, Radio Frequency (RF) and baseband hardware, and power and cooling equipment acquisition. As for OPEX increase, site rental and power consumption are among the most meaningful.

In traditional distributed RAN architecture, RF and baseband processing hardware is co-located in the cell site and not shared among different sites. Whereas in centralized RAN architectures, baseband processing is not only separated from RF processing hardware, i.e., remote radio heads (RRHs), but also centralized and it can be shared among different sites and even virtualized in Base Band Unit (BBU) pools [7]. Benefits from sharing BBU pools and statistical multiplexing in non-uniform traffic scenarios have been studied in [3], [8].

According to [9], centralized RAN architectures can be implemented in different variants, including BBU cloud. In this paper, we refer to Cloud Radio Access Network (C-RAN). In C-RAN, virtualized BBU pools running in virtual machines (VMs) are hosted in different central locations and can be flexibly configured and serve RRHs from various virtualized BBU pools each time. The authors in [10] presented a 3-layered logical structure for C-RAN taking advantage of computation in a cloud environment.

Because of the stringent requirements of the several interfaces needed in C-RAN and the maturity and evolution of different optical network technologies, optical networks have been proposed to support both, the fronthaul network connecting RRHs and BBUs, as well as the backhaul network connecting BBUs among them and to their peering point in the mobile core network. For the fronthaul, the authors in [11] proposed the use of Wavelength Division Multiplexing (WDM) technology and they reported a practical implementation with links up to 10 Gb/s interconnecting RRHs and BBUs. For the backhaul, Elastic Optical Networks (EON), as well as dynamic customer virtual networks (CVN) can be considered [12].

To interface the optical layer, there are several types of transponders that can be used in both, the front and the backhaul: *i*) Fixed Transponders (FT) that transmit at a fixed bitrate, e.g., 40Gb/s, *ii*) Bandwidth-Variable Transponders (BVT) that can adapt its bitrate up to a maximum capacity, e.g., 400Gb/s, and *iii*) Sliceable Bandwidth-Variable Transponders (SBVT) that can be shared among a number of optical connections.

So far, SBVTs have been proposed for core networks where every slice is used to support large capacity lightpaths, e.g., 100Gb/s and above [13], [14]. However, SBVTs can be

utilized in the metro segment (e.g., to support C-RAN) as long as they can provide finer granularity, e.g., 10-25 Gb/s. Specifically for C-RAN applications, such fine granularity would allow supporting both, the front and the backhaul networks.

In this paper, we first study in Section II RAN requirements in terms of dynamicity, granularity, and elasticity and the considered architecture model based on LTE. Next, in Section III, we review the state-of-the-art of SBVTs and conclude that no existing architecture fully supports the requirements for C-RAN applications. Given that, we propose an SBVT architecture based on Dynamic Optical Arbitrary Waveform Generation and Measurement (DOAWG/DOAWM) [15] that perfectly meets the requirements of these applications.

In Section IV, we propose a Mixed Integer Linear Programming (MILP) model for dimensioning locations hosting virtualized BBU pools (i.e., central offices, CO) to minimize CAPEX, while taking into account the different interfaces needed. Although the authors in [16] proposed an energy-efficient WDM aggregation network and formally defined the BBU placement optimization problem as an Integer Linear Programming (ILP) model aiming at optimizing the aggregation network in terms of power; and the authors in [17] have recently proposed an ILP model for optimal BBU hotel placement over WDM networks in centralized RAN, still few models can be found in the literature considering optical network equipment in C-RAN.

The proposed SBVT architecture is assessed in Section V. Next, the MILP model is used to compare FTs and the proposed SBVTs from the CAPEX perspective and to study the impact of the centralization level in C-RAN architectures in representative scenarios supported by optical networks. From the resulting CO design, impact of centralization level is also studied from the OPEX perspective, regarding network equipment power consumption.

II. Radio Access Networks

A. Distributed and Centralized RAN

Fig. 1 illustrates both distributed and centralized RAN architectures. In distributed RAN, RF and baseband hardware are co-located in the site and not shared with other sites, whereas, in centralized RAN, BBUs from different locations are co-located in the same BBU pool and can be shared between the various RRHs along the time.

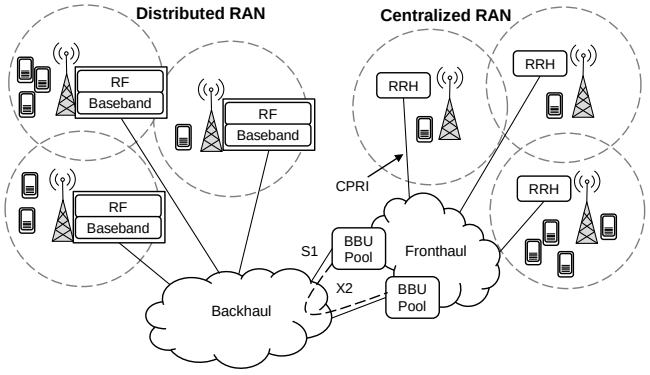

Fig. 1. Distributed and centralized RAN architectures.

From the mobile core network perspective, both distributed and centralized architectures require to interconnect base stations and their peering point through a backhaul network (e.g., MPLS over optical network). In addition to backhaul connections transporting user and control data (S1 interface), interconnection among neighboring cells' base stations may also be required (X2 interface). While latencies in the order of tens of milliseconds are allowed in S1 interfaces, tight coordination scheme between base stations led to maximum delays allowed in the order of hundreds of microseconds for the X2 interface thus, limiting the maximum distance between base stations requiring coordination.

Moreover, compared to distributed RAN, centralized RAN architectures require a fronthaul network aiming at providing connectivity between RRHs and BBUs in remote BBU pools and convey radio interface data. Among the different radio interface protocols, Common Public Radio Interface (CPRI) [18] is widely used; CPRI is a bidirectional protocol and its bitrate is constant and depends on the cell site configuration. Fig. 1 illustrates the logical links supporting CPRI, S1, and X2 interfaces in the centralized approach. In LTE and LTE-Advanced (LTE-A) technologies, CPRI requires not only huge capacity (in the order of Gb/s and tens of Gb/s), but also strict delay constraints (in the order of few hundreds μs round trip time, RTT).

B. C-RAN Architecture Model

In this paper, we consider a reference scenario based on the LTE and LTE-A technologies, where a set of geographically distributed RRHs cover certain regions and virtualized BBU pools are hosted in main COs. In addition, the peering point is located in a core CO, which hosts, among others, the mobility management entity (MME) and the serving gateway (S-GW) functions that in turn could be virtualized according to [7].

To provide the required capacity to support load fluctuations in different areas during the day, some of those RRHs can be activated or deactivated. Let us assume that activation (deactivation) of those RRHs can be done through the corresponding entity in charge of the control and management of the C-RAN. RRHs are connected to end-points through fiber links. To support CPRI links, connections from end-points to COs can be effectively implemented and dynamically modified, allowing a given RRH to be assigned to different virtualized BBU pools along the time. Moreover, to support handover and tight coordination schemes, among others, coordination among active and neighboring RRH needs to be considered; thus, X2 interfaces between virtualized BBUs in remote virtualized BBU pools are required. It is worth noting that, due to strict delay limitations required in X2 interfaces, not all BBUs in virtualized BBU pools in distant COs might be accessible among them. Finally, S1 links towards the core CO (hosting MME and S-GW) need also to be established over the backhaul network; we assume that the network is based on MPLS.

Fig. 2 depicts an example of the reference scenario where a set of RRHs corresponding to Macro Base Stations (MBS) cover large areas, and a set of small cells' RRHs cover smaller areas for capacity management according to the traffic

demand fluctuation at different hours. The next section faces the problem of minimizing CAPEX costs to equip main COs while satisfying demand at any time for all cells; CPRI, S1, and X2 interfaces requirements and limitations, such as capacity and maximum delay constraints, are considered.

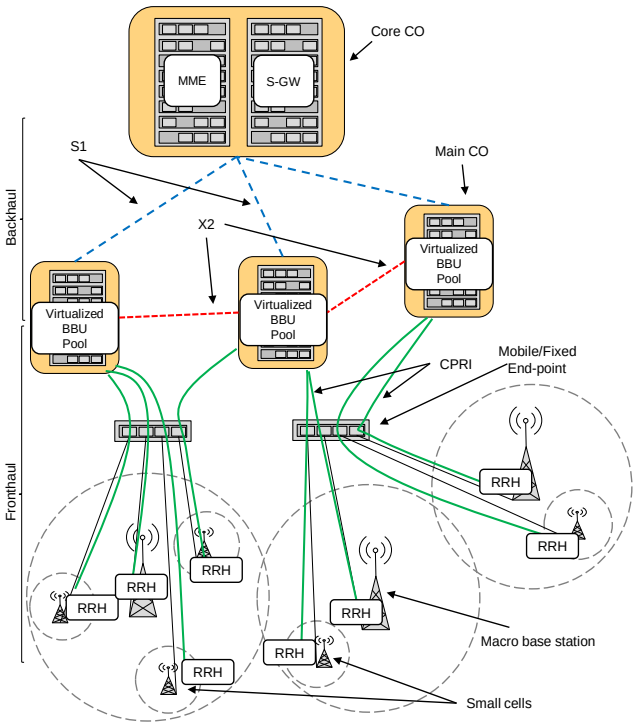

Fig. 2. An example of Cloud RAN architecture.

Different centralization levels of C-RAN will be studied in in this paper targeting at minimizing CAPEX regarding the cost needed to equip COs. Those centralization levels vary during the day to cope with the load that the network needs to serve.

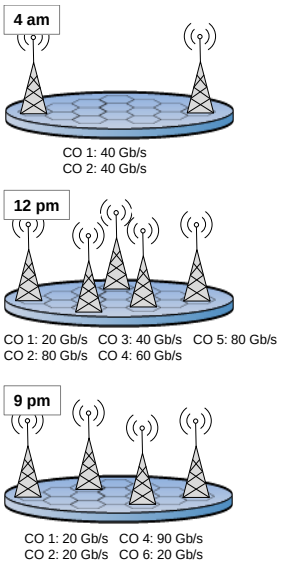

Fig. 3. Connections between COs and core-CO to support S1 interfaces.

For illustrative purposes, Fig. 3 presents the required connections between COs hosting BBU pools and the core-CO hosting both the MME and the S-GW for three representative hours of the day considering two different traffic profiles (business and residential); connections' capacities to support S1 interfaces are also shown.

At 4 am (off-peak period for both business and residential traffic profiles), active RRHs can be served from BBU pools hosted in two COs (COs 1 and 2). However, during peak business hour, at 12 pm, additional RRHs corresponding to small cells need to be activated. Interestingly, new BBU pools (hosted in COs 3, 4 and 5) are used to serve all the active RRHs at that time; connections' capacity fluctuations between COs 1 and 2 and the core-CO are as well observed. Similarly, during residential peak hour, at 9 pm, the BBU pool in CO 6 is used in addition to BBU pools in COs 1, 2 and 4. However, no RRHs are served from COs 3 and 5 and thus no connection is required between them and the core-CO. Compared to connections' capacities at 12 pm, fluctuations in the required capacity between COs 2 and 4 and the core-CO can be observed.

As a consequence, C-RAN clearly requires dynamic, elastic, and fine granularity (ranging from 10 Gb/s to 100 Gb/s) optical connections.

III. SBVT Architecture enabling 5G Mobile Networks

A. SBVT Architectures

As a key component of EONs, SBVTs implement a range of functions, including support of multiple bit rates (e.g., from 10 Gb/s to 1 Tb/s) and dynamically changeable modulation formats and baud rates. To increase the flexibility of EONs, SBVTs include multiple sub-transponders [14]. This capability enables flexibility using two methods: *i*) by freely configuring the modulation format of each sub-carrier and *ii*) by enabling the operation of each sub-carrier either as a single-carrier transponder or as part of a larger superchannel through the logical separation of flows with different destinations [13], [14].

Several studies conducted on the use of SBVTs show the numerous benefits that can be achieved. The common conclusion is that thanks to its flexibility, SBVTs have attractive features in terms of programmable rate per destinations, cost reduction when migrating towards high rate superchannels, and prospects for the integrability of several transponder elements into a single chip [14], [19].

At the physical layer, SBVTs can be implemented using coherent optical orthogonal frequency division multiplexing (CO-OFDM), coherent optical WDM (CO-WDM), Nyquist WDM [20], or DOAWG/DOAWM technologies.

The key element inside the SBVT is the optical front-end, which is the module distributing different traffic demands over several sub-carriers, which are then grouped into superchannels. The front-end contains a set of sub-carrier generation modules. The sub-carrier generation module consists of either an array of independent laser sources (multi-source as in Nyquist-WDM) or a single multi-wavelength source (i.e., a source able to generate several optical carriers from a single laser) as in the cases of CO-WDM or DOAWG/DOAWM. In the former case, all laser sources are independent, i.e., their central frequency can be configured to any value within the *C*-band and without additional constraints. In the latter case, the frequencies within the multi-

wavelength source are not independent, and thus, they have to be contiguous with a spectral separation typically limited within few tens of GHz. However, a multi-wavelength source can be less expensive and guarantees more stability than independent laser sources, hence, enabling better subcarrier spacing when the sliceable capability is not exploited (i.e., all sub-carriers are co-routed and contiguous), in turn guaranteeing higher spectral efficiency [14], [19].

Whereas all of the SBVT implementations mentioned above can cope with the requirements for superchannels generation, most of them lack the flexibility to accommodate efficiently fine granularity connections (e.g., 10 Gb/s). To cope with the dynamic, elastic, and fine granularity C-RAN scenarios' connection requirements, it is important that SBVTs be capable of fully exploiting the flexibility of EON networks. This means that, apart from generating superchannels, it is necessary to provide the feature of generating more channels than subcarriers when the connection requests are as slow as 10 Gb/s (or even slower), to optimize the SBVT capacity utilization.

B. DOAWG-based SBVT Architecture

The capability of DOAWG to arbitrarily shape a waveform in time and frequency by Fourier synthesis and by a combination of multiple spectral slices makes it possible to implement the SBVT functionality and requirements discussed previously naturally. For instance, Fig. 4 shows a DOAWG-based SBVT generating multiple channels of different bandwidth and modulation formats directed to different destinations.

Note that, the digital signal processing (DSP) for DOAWG allows generation of subchannels as well as superchannels (see Fig. 4) according to the connection requirements. In particular, as shown in Fig. 4 (center and bottom), the number of optical channels is not limited by the number of frequency comb lines and it is possible to generate a number of optical channels greater than the number of comb lines and spectral slices. This allows a more efficient and flexible utilization of the SBVT capacity and avoids the need for grooming finer connections since it can generate a channel as narrow as requested. This is not possible when using Nyquist WDM or coherent WDM. Finally, it is important to point out that the DOAWG DSP usually applies to subgroups of comb lines and spectral slices, as shown in Fig. 4. This guarantees that it is possible to redo the DSP for some spectral slices without affecting neighbors' channels (so that the reconfiguration can be hitless). Fig. 4 shows that the reconfiguration going from four channels in Fig. 4a to three channels in Fig. 4b and five channels in Fig. 4c affects only the first two DOAWG spectral slices.

DOAWG-based SBVT can be implemented using high-speed field programmable gate array (FPGA) and digital-to-analog converters (DAC), along with other optical front-end components (optical frequency combs (OFC), modulators, wavelength selective switch (WSS)). The FPGA and DACs form the electric core of the SBVT, which corresponds to the generation of sub- and superchannels. Fig. 5a shows the schematic diagram of a two slices SBVT – Electric Core (SBVT-EC). It maps a high-volume data sequence, like the 400 Gbit/s Cisco client interface, into multiple sub- and superchannels according to the NC&M functions. The NC&M tell the SBVT how many subchannels are needed to be provided and the required baudrate and modulation format for each of them. Once the number of subchannels and the baudrate/modulation is decided, similar to the conventional subcarrier multiplexing, the target waveform can be calculated through Tx DSP, which includes symbol mapping, data-rate adjusting, filtering, and frequency shifting [21]. The FPGA

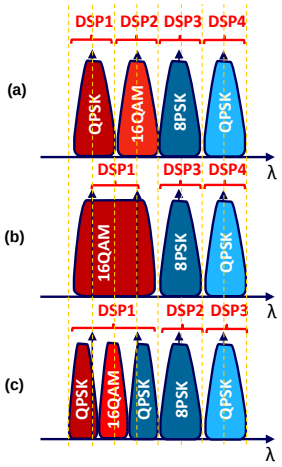

Fig. 4. Examples of multiple channels generated with one DOAWG-based SBVT with four comb-lines (spectral slices).

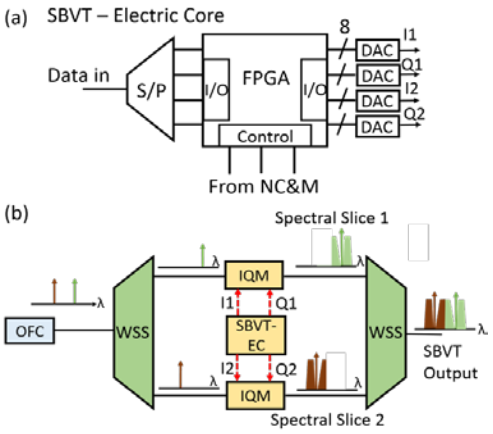

Fig. 5. Schematic diagram of the SBVT (a) and system diagram for two-slice SBVT generation (b).

then, sends the time-domain samples of the target waveform to DACs for waveform generation. Fig. 5b presents the system diagram for the two slices SBVT generation. We select two tones from the OFC using WSS and send them into two IQ modulators. Two complex outputs (I1/Q1 and I2/Q2) from the SBVT-EC are utilized to drive the two modulators, forming two phase-coherent spectral slices. The second WSS combines the two slices to create large-bandwidth superchannel.

IV. The C-RAN CAPEX Minimization (CRAM) Problem

Once the DOAWG-based SBVT has demonstrated its feasibility and applicability to C-RAN scenarios, let us focus on the C-RAN CAPEX minimization (CRAM) problem for dimensioning CO locations to minimize CAPEX. In line with

other network CAPEX minimization problems (e.g. see [22]), the CRAM problem assumes a known capacity to be provided.

A. Problem statement

The CRAM problem can be formally stated as follows:

Given:

- A set of geographically distributed RRHs H; representing $N(h)$ the subset of RRHs neighbouring RRH h; i.e. near RRHs operating at the same frequency band and requiring X2 interface links between them to interconnect their respective BBUs, and representing $H(t)$ the subset of H with the RRHs to be activated at time t.
- The tuple $<\alpha_h, \beta_h, \gamma_h>$ representing the required capacity by RRH h for CPRI, S1, and X2 interfaces respectively, in the case it is active. Since required capacity is constant and depends on the configuration, it can be pre-computed in advance.
- A set V of VMs' configurations with capabilities for BBU pools virtualization; each VM configuration v is defined by its cost κ_v and its number of BBUs it can virtualize λ_v; let us assume that one BBU can serve one RRH.
- A set of transponders P; each transponder p consists of a set of DSP modules $D(p)$, where the capacity of each module is φ_p and its cost κ_p; since gray or colored transponders may be considered to support the different interfaces, the parameters δ_p^{CPRI}, δ_p^{S1}, δ_p^{X2} indicate if p can support CPRI, S1 or X2 interface links respectively.
- A set of line cards C; each line card c can support one type of transponder, and it is defined by its cost κ_c and the number of ports to plug-in transponders ξ_{cp}.
- A set of MPLS equipment E; each switch e is defined by its cost κ_e, its switching capacity σ_e, and the number of available slots ρ_e to plug-in line cards; the parameter η_{ec} represents if equipment e can support card c.
- A set O with main COs; each main CO can be equipped with a predefined configuration of VMs and with a MPLS switch.
- $O(h)$ represents the subset of main COs that can be reached by RRH h without exceeding delay imposed by CPRI requirements.
- $U(o)$ accounts for the subset of main COs that can be reached from main CO o without violating X2 delay constraints.
- A core CO with functions for MME, S-GW, along with others.

Output: the VMs' configurations and MPLS equipment, lines cards and transponders to install in each main CO.

Objective: minimize the cost of VMs' configurations, MPLS equipment, line cards and transponders used.

B. Mathematical model

The following sets and parameters have been defined:

H	Set of RRHs.
O	Set of main COs.
V	Set of VMs' configurations that can be equipped in main COs.
E	Set of MPLS equipment that can be equipped in main COs.
T	Set of hours.
P	Set of transponders.
$D(p)$	Set of DSP modules of transponder p
C	Set of line cards types.
$H(t)$	Subset of H with RRHs active at time t.
$N(h)$	Subset of H with RRHs neighboring h.
$O(h)$	Subset of O with main COs that can be accessed by RRH h without exceeding the CPRI delay constraint.
$U(o)$	Subset of O with main COs that can be reached from main CO o without exceeding the X2 delay constraint.
λ_v	Number of VMs in VMs's configuration v.
α_h	Capacity required in CPRI link by RRH h in the case of being active.
β_h	Capacity required in S1 interface link by RRH h in the case of being active.
γ_h	Capacity required in X2 interface link by RRH h in the case of being active.
φ_p	Capacity of DSP module of transponder p.
δ_p^{CPRI}	1 if transponder p can support CPRI links.
δ_p^{S1}	1 if transponder p can support S1 interface links.
δ_p^{X2}	1 if transponder p can support X2 interface links.
ξ_{cp}	Number of ports in line card type c to support transponder p; 0 if line card type c does not support transponder p.
σ_e	Available capacity in equipment e.
ρ_e	Number of available slots in equipment e.
η_{ec}	1 if equipment e can support line card type c; 0 otherwise.
κ_v	Cost of VM configuration v.
κ_p	Cost of transponder p.
κ_c	Cost of line card type c.
κ_e	Cost of equipment e.
$bigM$	Large positive constant.

Decision variables:

x_{ov}	Binary. 1 if CO o is equipped with VM configuration v; 0 otherwise.
y_{oe}	Binary. 1 if CO o is equipped with equipment e; 0 otherwise.
l_{oc}	Integer. Number of cards of type c to equip in o.
a_{op}	Integer. Number of transponders p in CO o.
z_{hot}	Binary. 1 if RHH h is assigned to CO o at time t; 0 otherwise.
$w_{hoo't}$	Integer. Number of X2 interface links required between COs o and o' by RRH h at time t.
r_{hotpd}	Binary. 1 if DSP module d in transponder p is used in main CO o to support CPRI links at time t for RRH h; 0 otherwise.

q_{hotp} Binary. 1 if transponder p is equipped in main CO o to support CPRI links at time t for RRH h; 0 otherwise.

m_{otp} Integer. Number of transponders p to equip in main CO o to support S1 interface links at time t.

$n_{oo'tp}$ Integer. Number of transponders p to equip in CO o to support X2 interface links at time t to reach CO o'.

The problem can be formulated as follows:

$$\text{Minimize} \quad \sum_{o\in O}\sum_{v\in V}\kappa_v \cdot x_{ov} + \sum_{o\in O}\sum_{e\in E}\kappa_e \cdot y_{oe} + \sum_{o\in O}\sum_{c\in C}\kappa_c \cdot l_{oc} + \sum_{o\in O}\sum_{p\in P}\kappa_p \cdot a_{op} \tag{1}$$

subject to:

$$\sum_{o\in O(h)} z_{hot} = 1 \quad \forall t\in T, h\in H(t) \tag{2}$$

$$\sum_{v\in V}\lambda_v \cdot x_{ov} \geq \sum_{h\in H(t)} z_{hot} \quad \forall t\in T, o\in O \tag{3}$$

$$\sum_{v\in V} x_{ov} \leq 1 \quad \forall o\in O \tag{4}$$

$$w_{hoo't} \geq \sum_{h'\in N(h)} z_{h'o't} - (1-z_{hot})\cdot bigM \quad \forall t\in T, h\in H(t), o\in O(h), o'\in U(o) \tag{5}$$

$$\sum_{o'\in O\setminus U(o)}\sum_{h'\in N(h)} z_{h'o't} \leq (1-z_{hot})\cdot bigM \quad \forall t\in T, h\in H(t), o\in O \tag{6}$$

$$\sum_{p\in P}\varphi_p \cdot \delta_p^{CPRI} \cdot \sum_{d\in D(p)} r_{hotpd} \geq \alpha_h \cdot z_{hot} \quad \forall t\in T, h\in H(t), o\in O(h) \tag{7}$$

$$\sum_{o\in O}\sum_{p\in P}\sum_{d\in D(p)} r_{hotpd} = 1 \quad \forall t\in T, h\in H(t) \tag{8}$$

$$q_{hotp}\cdot |D(p)| \geq \sum_{d\in D(p)} r_{hotpd} \quad \forall t\in T, h\in H(t), o\in O(h), p\in P \tag{9}$$

$$\sum_{p\in P}\varphi_p \cdot |D(p)| \cdot \delta_p^{S1} \cdot m_{otp} \geq \sum_{h\in H}\beta_h \cdot z_{hot} \quad \forall t\in T, o\in O \tag{10}$$

$$\sum_{p\in P}\varphi_p \cdot |D(p)| \cdot \delta_p^{X2} \cdot n_{oo'tp} \geq \sum_{h\in H}\gamma_h \cdot w_{hoo't} \quad \forall t\in T, o\in O, o'\in U(o) \tag{11}$$

$$n_{oo'tp} = n_{o'otp} \quad \forall t\in T, o\in O, o'\in U(o), p\in P \tag{12}$$

$$a_{op} \geq \sum_{h\in H} q_{hotp} + m_{otp} + \sum_{o'\in U(o)} n_{oo'tp} \quad \forall t\in T, o\in O, p\in P \tag{13}$$

$$\sum_{e\in E} y_{oe} = \sum_{v\in V} x_{ov} \quad \forall o\in O \tag{14}$$

$$\sum_{c\in C}\xi_{cp} \cdot l_{oc} \geq a_{op} \quad \forall o\in O, p\in P \tag{15}$$

$$\sum_{e\in E}\rho_e \cdot y_{oe} \geq \sum_{c\in C} l_{oc} \quad \forall o\in O \tag{16}$$

$$\sum_{e\in E}\sigma_e \cdot y_{oe} \geq \sum_{p\in P}\alpha_p \cdot a_{op} \quad \forall o\in O \tag{17}$$

$$l_{oc} \leq \rho_e \cdot \eta_{ec} + (1-y_{oe})\cdot bigM \quad \forall o\in O, e\in E, c\in C \tag{18}$$

The objective function (1) minimizes the cost of the VM configurations, MPLS equipment, line cards and transponders to equip in main COs.

The first set of constraints deal with the assignment of RRHs to main COs. Constraint (2) ensures that RRHs are assigned to one and only one accessible main CO at each time when they are active. Constraint (3) guarantees that VM configuration selected in each main CO has enough VMs to satisfy BBU virtualization for the RRHs assigned to it, while constraint (4) makes sure that one VM configuration is assigned to a main CO at the most.

Constraint (5) allows accounting for the number of X2 interface links between main COs o and o' that are required for RRH h at time t. This inequality actually sets a lower bound on $w_{hoo't}$ if and only if RRH h is assigned to main CO o at time t. Constraint (6) guarantees that, if RRH h is assigned to main CO o, their neighboring RRHs are not assigned to COs that cannot be accessed from main CO o to guarantee that X2 interface links would not exceed delay constraint.

Constraints (7)-(13) are in charge of selecting the proper transponder configuration for each interface link. Specifically, constraints (7)-(9) guarantee that transponder p selected for CPRI link of active RRH h at t has enough capacity and that one and only one DSP module is selected. Constraint (10) ensures that capacity of transponders selected in main CO o for S1 interface links is enough to satisfy the total S1 interfaces' capacity required in o at each time. Similarly, constraint (11) ensures that capacity of transponders selected for X2 interface links between main COs is enough to satisfy the required capacity for X2 interfaces in o for every time. Constraint (12) ensures that the same transponders' configuration is selected for X2 interfaces between main COs o and o'. Constraint (13) accounts the number of transponders of each type to equip in main CO o to guarantee the required connections at any time.

Finally, constraints (14)-(18) deal with MPLS equipment at main COs. Constraint (14) ensures that a main CO is equipped only if it is active. Constraint (15) guarantees that the cards to equip in each main CO can support the selected transponders. Constraints (16) and (17) guarantee that the switching equipment selected has enough slots and capacity respectively. Finally, constraint (18) ensures that if MPLS equipment e is assigned to main CO o, and it does not support line card c, that line card is not equipped in o.

Considering the particular case where the exact number of main COs to equip is given, the parameter Φ representing the number of main COs to equip is defined and the model extended with the following constraints:

$$\sum_{t\in T}\sum_{h\in H(T)} z_{hot} \geq \sum_{e\in E} y_{oe} \quad \forall o\in O \tag{19}$$

$$\sum_{e\in E}\sum_{o\in O} y_{oe} = \Phi \tag{20}$$

Constraint (19) ensures that only main COs that host BBUs assigned to active RRHs at some time are equipped, whereas constraint (20) ensures that Φ main COs are equipped.

The amount of variables and constraints approximates to $|O|\cdot(|V|+|E|+|C|+|T|\cdot|P|\cdot(|H|+|O|))$ and $|T|\cdot|O|^2\cdot(|P|+|H|)$, respectively. Note that the amount of COs and RRHs highly impacts on the size of problem instances. The instances generated in this paper could be solved to optimality in

reasonable solving times (hours). Nonetheless, in case the size of the instances prevent form solving them to optimality, additional methods based on column generation [23] or randomized meta-heuristics [24] could be developed.

V. Results

In this section, we first focus on the assessment of the proposed DOAWG-based SBVT. Next, we apply the MILP model presented in the previous section to study CAPEX from installing FTs or SBVTs and from different centralization levels. Finally, OPEX is also studied.

A. DOAWG-based SBVT Assessment

To demonstrate the DOAWG-based SBVT described in Section III.B, we implemented the system described in Fig. 5b. Fig. 6 shows the two subcarriers generated from one single laser with 100 kHz linewidth to transmit three channels with QPSK modulation format.

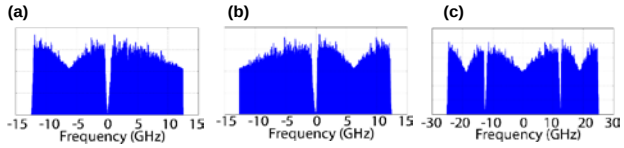

Fig. 6. Spectral slice 1 (a), 2 (b) and combined spectrum (c).

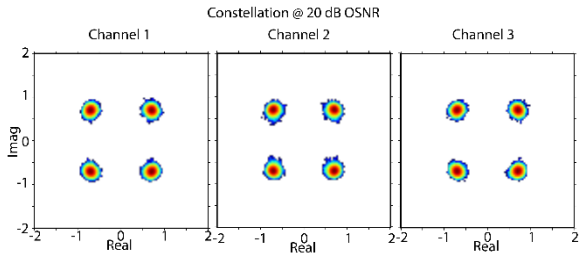

Fig. 7. Constellation plots for channel 1, 2 and 3 @ 20 dB OSNR.

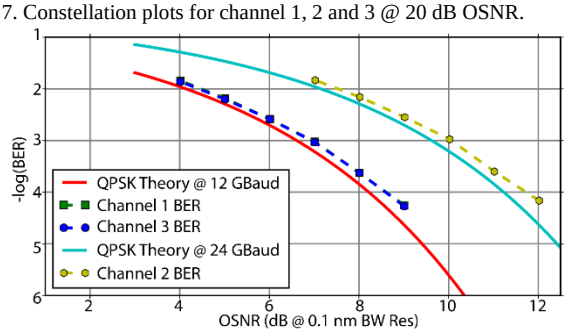

Fig. 8. BER vs. OSNR @ 0.1 dB bandwidth resolution for theoretical curves at 12 and 24 GBaud and channel 1, 2 and 3.

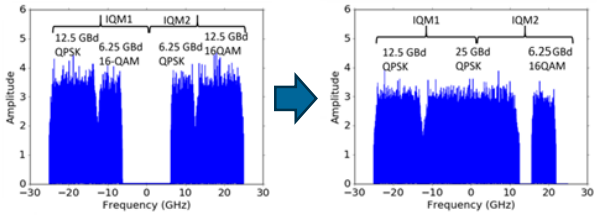

Fig. 9. SBVT reconfiguration from four channels to three channels configuration with one superchannel.

We select two tones from the optical frequency combs using WSS and send them into two different IQ modulators driven by the DACs with target spectra in Fig. 6a and Fig. 6b. Fig. 6c shows the spectrum after combination. The two tones are set to be 25 GHz apart. Channel 1 and channel 3 both carry 12 GBaud 2^{15}-1 PRBS signals and are shaped by a Nyquist filter with a roll-off factor of 1/24, and both occupy a bandwidth of 12.5 GHz. The center channel 2 is a 24 GBaud 2^{15}-1 PRBS signal with 25 GHz bandwidth shaped by the same Nyquist filter. For the receiver DSP, a 13-tap finite impulse response (FIR) based on constant modulus algorithm (CMA) [25] equalizes the linear distortion of the received waveform and adaptively updates the tap coefficients. Then, a 2-stage carrier frequency and phase recovery algorithm locks down the frequency offset and phase noise of the received waveform [26].

Fig. 7 shows the constellation at 20 dB optical signal-to-noise ratio (OSNR) after CMA and carrier phase recovery. Finally, we show bit error ratio (BER) vs. OSNR using 393,204 symbols. Fig. 8 shows the theoretical BER curves for 12 and 24 GBaud and BER results for the three different channels. We observe ~0.2 dB OSNR penalty at 10^{-3} BER, which is mainly due to the distortions from the sinusoidal transfer function of the IQ modulators and the laser phase noise.

Finally, let us show the SBVT ability to change its configuration. Fig. 9 shows calculated target waveforms for two scenarios where the SBVT is configured to generate four and three subchannels/superchannels with different baudrate and modulation formats using low-speed electronic and optoelectronic devices (25 GS/s DACs and 25 GHz IQMs). A comprehensive theory and experimental demonstration of the SBVT generation can be found in [27].

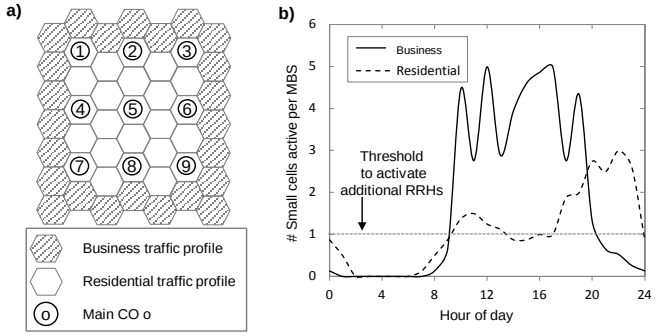

Fig. 10. Cells and main CO placement (a) and number of small cells active, per MBS, against the hour of day (b).

B. CAPEX and OPEX studies

Once that the DOAWG-based SBVT has been assessed, let us focus on studying the resulting CAPEX and OPEX from different centralization levels. For evaluation purposes, we consider a scenario where 49 RRHs, e.g., representing MBSs, are geographically distributed covering an area of about 500 km^2. The outmost cells cover regions where the traffic load varies according to business load profile, and the central ones vary according to a residential profile similarly as described in [3], e.g., representing an urban area surrounded by industrial zones; Fig. 10a depicts the reference scenario. To guarantee delay constraints in such scenario, sets $O(h)$ and $U(o)$ in the MILP model are defined based on distances among locations.

In addition, a set of RRHs, e.g., corresponding to small cells, are also geographically distributed for capacity

management resulting thus, in a scenario with 195 RRHs; it is worth highlighting that not all of them will be active simultaneously since the traffic profiles vary differently along the day. Nonetheless, MBSs' RRHs are always considered active to guarantee coverage even in off-peak hours; whereas small cells' RRHs are progressively activated (deactivated) as load increases (decreases). Fig. 10b illustrates the number of active small cells' RRHs per MBS required for the two profiles against hour of day. A set of main COs that can be selected to host virtualized BBU pools is considered. Their location is illustrated in Fig. 10a. We target a maximum 150 μs RTT between RRHs and BBUs and, as a consequence, no single main CO can be accessed by all RRHs in the evaluated scenarios. One sector is considered in each cell.

CAPEX is studied from the network equipment perspective (MPLS switches, line cards, and transponders to equip in main COs) considering two different types of transponders (FTs and the proposed SBVTs) and for different centralization levels. The network equipment's cost is based on the cost model in [28], while a multiplicative cost is used for the SBVTs [29]. Virtualized BBU pools' cost is not considered since computers' cost is much lower than that of the transponders and switches. The MILP model described in the previous section was implemented, and several instances were solved using CPLEX.

For the CAPEX studies, we firstly consider different configurations based on the previously described scenario and solve problem instances for peak hours.

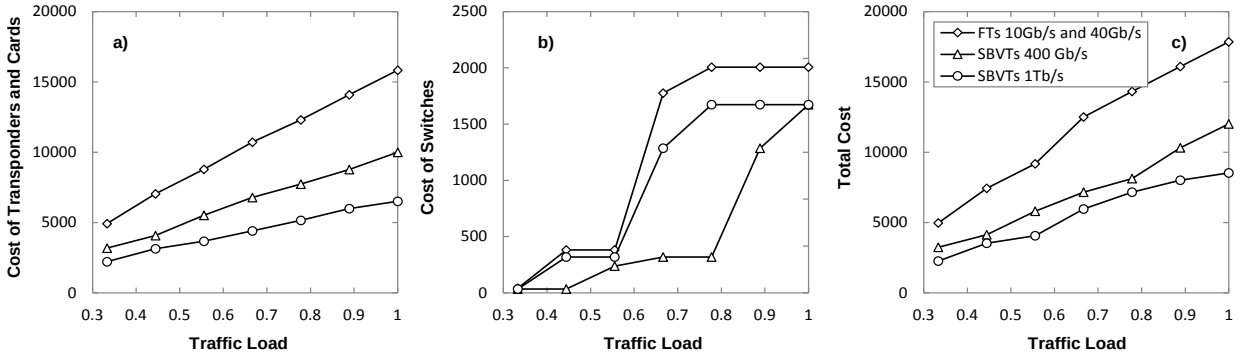

Fig. 11. Transponders (a), Switches (b) and Total cost (c) as a function of the normalized network load when 10Gb/s and 40Gb/s FTs, 400Gb/s, or 1Tb/s SBVTs are installed.

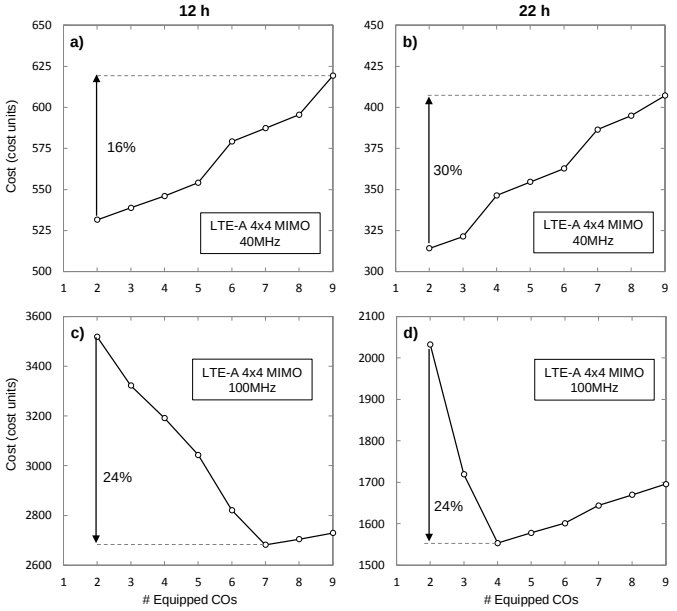

Fig. 12. Cost evolution against the number of main COs to equip for two different LTE-A configurations at 12h and 22h.

Aiming at comparing CAPEX when using FTs and SBVTs, graphs in Fig. 11 present the cost (in terms of cost units, where 1 cost unit is the cost of a 10 Gb/s transponder, [28]) against network load of installing 10Gb/s and 40Gb/s FTs, 400Gb/s, or 1Tb/s SBVTs in the switches. As shown, the total cost is dominated by the cost of the transponders, where the cost savings obtained are around 35% and 50% from installing 400Gb/s and 1Tb/s SBVTs, respectively, with respect to the cost of installing FTs. In addition, there are savings coming from the smaller size of the installed MPLS switches as a result of the reduction in the number of slots that are needed when SBVTs are considered. This is especially noticeable in the case of adopting 400Gb/s SBVTs.

Aiming at studying CAPEX for different centralization levels, let us now consider different peak and off-peak hours. We assume two different LTE-A 4x4 Multiple Input Multiple Output (MIMO) [30] configurations: *i*) 40MHz requiring CPRI links' capacity close to 10Gb/s and S1 and X2 links' capacity about 600 Mb/s and 230 Mb/s, respectively, and *ii*) 100MHz requiring CPRI links' capacity close to 25 Gb/s and S1 and X2 links' capacity about 1.5 Gb/s and 550 Mb/s, respectively [31].

Fig. 12 shows the network equipment cost evolution against the number of main COs to equip for peak hours in business (12 h) and residential areas (22 h) and for LTE-A 4x4 MIMO 40MHz (Fig. 12a and b) and LTE-A 4x4 MIMO 100MHz (Fig. 12c and d) configurations. The maximum centralization level requires two main COs since this is the minimum number of COs required to support all RRHs without exceeding delay constraints. Indeed, for the 40MHz configuration (Fig. 12a and b), equipping the same 2 COs at any time with the cheapest equipment configuration, results in the minimum cost solution.

Interestingly, as soon as CPRI links' capacity increases (Fig. 12c and d), e.g., due to a configuration upgrade from 40MHz to 100MHz, the number of main COs to equip with minimum cost moves away from the fully centralized solution at peak hours. Results for off-peak hours showed that the fully centralized case, 2 COs, satisfies the demand at that time and

with the minimum cost. As it can be seen in Fig. 12c and d, equipping more than 7 and 4 COs at the corresponding peak hours, increases the cost.

Considering the 100MHz configuration and aiming at dimensioning our scenario, we restricted the set of COs that can be selected to 7 main COs, corresponding to the ones that need to be equipped to satisfy demand at peak hours and that can be selected to satisfy demand at any time. The problem was solved for each hour separately, and the minimum cost solutions obtained were saved. Then, each main CO was dimensioned with the minimum equipment to satisfy demand at any hour. Although the proposed mathematical model can solve the problem considering all hours of day jointly, splitting the problem into different instances per each hour allows solving it in reasonable times, while obtaining good enough solutions as it will be seen in the next paragraphs. Results showed that by equipping seven main COs with the smallest MPLS switches, demand is satisfied at any time. More specifically, the required equipment to be installed resulted in 2867.6 cost units in terms of CAPEX.

Similarly, we dimensioned the same configuration scenario considering the fully centralized approach, where only 2 COs can be equipped, and a theoretical fully distributed approach, where 49 main COs are equipped, each to serve a single MBS' RRH and its small cells' RRHs. From the results, the fully centralized approach required a huge capacity switch (6.72 Tb/s and 48 slots) and a small one (2.24 Tb/s and 16 slots), whereas the fully distributed required 49 of the smallest switch (1.40 Tb/s and 10 slots). CAPEX value obtained for the fully centralized approach was 3518.4 cost units, whereas for the fully distributed one, was 4694.9 cost units. The solution obtained when 7 COs were equipped, represents CAPEX savings as high as 18% and 39% compared to the scenarios where 2 and 49 COs were equipped respectively.

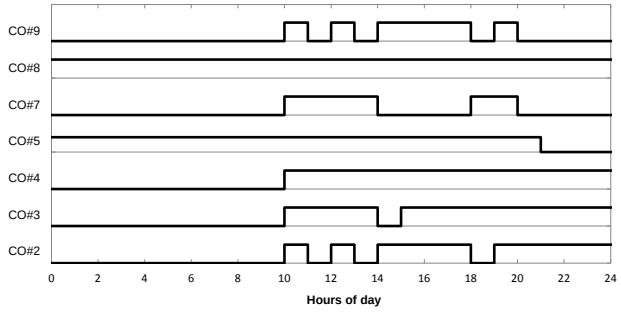

Fig. 13. Main COs to equip against hours of day.

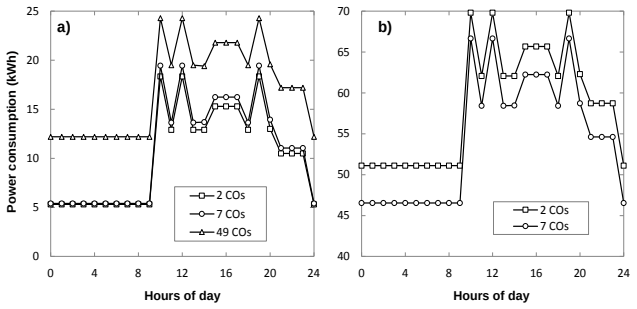

Fig. 14. Power consumption of transponders (a) and total equipment (b).

Focusing on the main COs to equip hour by hour, Fig. 13 illustrates that during off-peak hours only two COs need to be equipped whereas for peak hours, more main COs need to be equipped. An elastic CO network equipment use is envisioned.

For completeness, we also study the impact of the centralization level taking into account the power consumption of the equipment along the day.

In line with [32], we assume that the power consumption of switches can be approximated as the summation of the consumption of the basic node, the slots cards, and the port cards. In addition, we consider a fixed component of power consumption in MPLS switches related to the basic node and its slots power requirements and a variable contribution from the line cards and transponders in use, assuming that they only consume when they are in use.

Fig. 14 represents the power consumption of transponders (Fig. 14a) and total power consumption considering all the equipment in all the main COs (Fig. 14b) against day hours. As expected, since the fully centralized approach is the one requiring the lowest number of transponders to be equipped, their contribution to the power consumption is also the lowest. On the contrary, the distributed approach is the one requiring more transponders, since each main CO requires the necessary equipment not only for the CPRI interfaces but also for the X2 and S1 interfaces. The solution requiring 7 COs to be equipped, results in a slight increment of 5% in terms of transponders' power consumption compared to the centralized approach, and savings near 37% in relation to the distributed one. Notwithstanding, the contribution of switches and line cards to power consumption needs to be considered to evaluate OPEX.

As described in the CAPEX study, because of the equipment selection for CAPEX minimization, the centralized approach requires a huge capacity switch plus a small one, and the distributed approach requires 49 units of the smallest switches. For the centralized approach, it is clear that the high power consumption of the large switch will impact the total power consumption, even though, the lowest number of transponders is required. As shown in Fig. 14b, the centralization level requiring 7 COs presents lower total power consumption than the fully centralized approach; savings close to 7% are observed. Values for the fully distributed approach are not depicted in Fig. 14b, since computing only the fixed contribution from the 49 smallest switches is as high as 270 kWh (49 x 5.51 kWh). The 7 COs solution shows savings close to 82% compared to the fully distributed approach.

Finally, as showed in Fig. 14a, it is clear that for any of the approaches considered, equipment usage follows curves along day hours similarly as traffic load figures shown in Fig. 10.

VI. Conclusions

The connectivity requirements for C-RAN scenarios were studied in terms of dynamicity, elasticity, and granularity. Although different SBVT implementations have been proposed, no one fulfills C-RAN requirements regarding fine spectrum granularity. Hence, DOAWG as candidate for implementing SBVTs was introduced, since it enables flexibility in the temporal and spectral domains by combining

multiple spectral slices and generating optical channels with subwavelength granularity as well as superchannels. The sliceabilty is not limited by the number of combs, making DOAWG based SBVT exceptionally flexible and adaptable to any type of optical channel. In particular, it was shown the DOAWG's fine granularity capability by generating optical channels of 6.25GHz and 12.5GHz in a single comb line.

To perform CAPEX and OPEX studies and assuming that C-RAN is supported by optical networks, the CRAM problem for C-RAN CAPEX minimization has been presented and formally defined using a MILP model. The mathematical model was implemented and problem instances considering different centralization levels and LTE-A configurations were solved using CPLEX.

Results showed that remarkable cost savings can be obtained when installing the proposed SBVTs compared to installing fixed transponders.

Next, the impact of the centralization level in optical network-supported C-RAN was studied. Results showed that, in the evaluated scenarios, although the maximum centralization level results in the minimum CAPEX solution for certain LTE-A configuration, as soon as higher capacities are required in different LTE-A interfaces (e.g. due to a configuration upgrade) lower levels of centralization result in CAPEX savings up to 18% compared to the fully centralized approach. Savings as high as 39% were observed compared to a fully distributed approach.

For completeness, OPEX was also studied from the solutions obtained after solving the CRAM problem. OPEX savings near 7% and up to 82% were shown for the solution requiring a low level of centralization compared to the fully centralized and fully distributed approaches respectively.

ACKNOWLEDGEMENTS

The research leading to these results has received funding from the Spanish MINECO SYNERGY project (TEC2014-59995-R), from the Catalan Institution for Research and Advanced Studies (ICREA), from DOE under grant DE-FC02-13ER26154, from NSF under EECS grant 1028729, and from ARL under grant W911NF-14-2-0114.

REFERENCES

[1] A. Asensio et al., "Study of the Centralization Level of Optical Network-Supported Cloud RAN," in Proc. ONDM, 2016.

[2] Y. Lin, et al., "Wireless network cloud: Architecture and system requirements," IBM J. of Research and Development, vol.54, no.1, pp.4:1-4:12, 2010.

[3] "C-RAN the road towards green RAN," China Mobile Research, 2011.

[4] "Cisco Visual Networking Index: Global Mobile Data Traffic Forecast Update, 2014–2019," CISCO Whitepaper, 2015.

[5] I. Chih-Lin, et al., "Recent Progress on C-RAN Centralization and Cloudification," IEEE Access, vol.2, no., pp.1030-1039, 2014.

[6] A. Checko, et al., "Cloud RAN for Mobile Networks—A Technology Overview," IEEE Comm. Surveys & Tutorials, vol.17, pp.405-426, 2015.

[7] L. Velasco, et al., "A service-oriented hybrid access network and clouds architecture," IEEE Comm. Magazine, vol.53, pp.159-165, 2015.

[8] A. Checko, H. Holm, and H. Christiansen, "Optimizing small cell deployment by the use of C-RANs," in Proc. of European Wireless 2014, 20th European Wireless Conference, pp.1-6, 2014.

[9] T. Pfeiffer, "Next generation mobile fronthaul and midhaul architectures," IEEE/OSA J. of Optical Comm. and Netw., vol.7, pp. B38-B45, 2015.

[10] W. Jun, et al., "Cloud radio access network (C-RAN): a primer," IEEE Network, vol.29, no.1, pp.35-41, 2015.

[11] F. Ponzini, et al., "Centralized radio access networks over wavelength-division multiplexing: a plug-and-play implementation," IEEE Comm. Magazine, vol.51, no.9, pp.94-99, 2013.

[12] A. Asensio et al., "Dynamic Virtual Network Connectivity Services to Support C-RAN Backhauling," IEEE/OSA Journal of Optical Communications and Networking (JOCN), vol. 8, pp. B93-B103, 2016.

[13] A. Napoli et al., "Next generation elastic optical networks: The vision of the European research project IDEALIST," IEEE Commun. Mag., vol. 53, pp. 152-162, 2015.

[14] N. Sambo et al., "Next generation sliceable bandwidth variable transponders," IEEE Commun. Mag, vol. 53, pp. 163-171, 2015.

[15] R. P. Scott et al., "Dynamic optical arbitrary waveform generation and measurement," Optics Express, vol. 18, pp. 18655-18670, 2010.

[16] N. Carapellese et al., "Energy-Efficient Baseband Unit Placement in a Fixed/Mobile Converged WDM Aggregation Network," IEEE J. on Selected Areas in Communications, vol.32, no.8, pp.1542-1551, 2014.

[17] F. Musumeci et al., "Optimal BBU placement for 5G C-RAN deployment over WDM aggregation networks," J. of Lightw. Tech., vol. 34, pp. 1963-1970, 2016.

[18] http://www.cpri.info/downloads/CPRI_v_7_0_2015-10-09.pdf

[19] N. Sambo et al., "Sliceable transponder architecture including multiwavelength source," J. of Optical Commun. and Networking, vol. 6, pp. 590-600, 2014.

[20] G Bosco et al., "On the performance of Nyquist-WDM terabit superchannels based on PM-BPSK, PM-QPSK, PM-8QAM or PM-16QAM subcarriers," J. of Lightwave Technol., vol. 29, pp. 53-61, 2011.

[21] M. Qiu et al, "Digital subcarrier multiplexing for fiber nonlinearity mitigation in coherent optical communication systems," Opt. Express vol. 22, pp. 17770-18777, 2014.

[22] O. Pedrola, A. Castro, L. Velasco, M. Ruiz, J. P. Fernández-Palacios, D. Careglio, "CAPEX study for Multilayer IP/MPLS over Flexgrid Optical Network," IEEE/OSA Journal of Optical Communications and Networking (JOCN), vol. 4, pp. 639-650, 2012.

[23] M. Ruiz, M. Pióro, M. Zotkiewicz, M. Klinkowski, and L. Velasco, "Column Generation Algorithm for RSA Problems in Flexgrid Optical Networks," Springer Photonic Network Communications, vol. 26, pp. 53-64, 2013.

[24] O. Pedrola, M. Ruiz, L. Velasco, D. Careglio, O. González de Dios, and J. Comellas, "A GRASP with path-relinking heuristic for the survivable IP/MPLS-over-WSON multi-layer network optimization problem," Elsevier Computers & Operations Research (COR), vol. 40, pp. 3174-3187, 2013.

[25] D. Godard, "Self-Recovering Equalization and Carrier Tracking in Two-Dimensional Data Communication Systems," Transactions on Commun., vol. 28, pp. 1867-1875, 1980.

[26] D.-S. Ly-Gagnon et al., "Coherent Detection of Optical Quadrature Phase-Shift Keying Signals with Carrier Phase Estimation," J. Lightwave Technol., vol. 24, pp. 12-21, 2006.

[27] R. Proietti et al, "Elastic Optical Networking by Dynamic Optical Arbitrary Waveform Generation and Measurement," J. of Optical Commun. and Networking, vol. 8, pp. A171-A179, 2016.

[28] F. Rambach et al., "A multilayer cost model for metro/core networks," IEEE/OSA J. of Optical Comm. and Netw., vol.5, pp.210-225, 2013.

[29] L. Velasco, O. González de Dios, V. López, J. Fernández-Palacios, and G. Junyent, "Finding an Objective Cost for Sliceable Flexgrid Transponders," in Proc. OFC, 2014.

[30] D. Gesbert et al., "Shifting the MIMO Paradigm," IEEE Signal Processing Magazine, vol. 24, no. 5, pp. 36-46, Sep. 2007.

[31] EU COMBO project, "Deliverable D3.3 Analysis of transport network architectures for structural convergence," 2015.

[32] W. Van Heddeghem et al., "Power consumption modeling in optical multilayer networks," Photonic Netw. Comm., vol. 24, pp 86-102, 2012.